electronics

MDPI

Article

Theoretical Analysis of the Time Transient of the THz Self-Mixing Rectification Voltage in a Semiconductor Barrier

Fabrizio Palma

Dipartimento di Ingegneria dell'Informazione, Elettronica e Telecomunicazioni, Università di Roma La Sapienza, 00185 Roma, Italy; fabrizio.palma@uniroma1.it

Abstract: THz detection in a silicon structure can be an effective instrument not only for image detection, and material and gas sensing, but also for communications. Next-generation 6G communications assume the possibility of achieving a large-band transmission, using free space propagation with THz carriers. This possibility relies on the availability of an effective, low-cost detector technology. THz detection by self-mixing can provide an effective amplitude demodulation of the incoming carrier, with antennas directly fabricated on the chip. In this case, the speed of the detectors represents a crucial point in the definition of the bandwidth whereby several GHz are indeed required by the communication systems. The self-mixing process is intrinsically very fast, since it depends on the non-linear interaction of the radiation with the majority carriers inside the semiconductor structure. In this paper, we evaluate analytically the time dependence of the onset of the rectified voltage. A potential propagation along the detector channel follows the self-mixing rectification, accompanied by the charging of the parasitic capacitances of the structure. A numerical simulator can easily evaluate the delay due to this propagation along the structure, but the transient of the true origin of the signal, i.e., the establishment of the self-mixing voltage, at the current time, can be only inferred by analytical approach. In this work, we use the model developed for the THz rectification in the depletion region of an MOS capacitance to develop a transient model of the formation of the characteristic self-mixing charge dipole, and of the generation of the rectified potential. Subsequently, we show by TCAD simulations the propagation of the effect on the semiconductor structure, which surrounds the rectifying barrier, and evaluate the overall time response of a detector.

Keywords: terahertz radiation; transient detection; semiconductor device modeling

Citation: Palma, F. Theoretical Analysis of the Time Transient of the THz Self-Mixing Rectification Voltage in a Semiconductor Barrier. *Electronics* **2023**, *12*, 1264. https://doi.org/10.3390/electronics12061264

Academic Editors: Anirban Das and Briliant A. Prabowo

Received: 28 January 2023
Revised: 2 March 2023
Accepted: 3 March 2023
Published: 7 March 2023

1. Introduction

Extensive literature demonstrates that CMOS technology can be suitable for the realization of the THz detector, with very high sensitivity. Recent results showed in particular that a high transmission velocity can be achieved using a proper detection architecture [1–3]. These results, combined with the intrinsic low cost of the CMOS technology, allows us to foresee this as a suitable solution for the large market of the future 6G communication systems.

The detection of high-frequency electromagnetic radiation using integrated commercial electronics, in particular, terahertz (THz) radiation, represents a challenging task that is pushing significant experimental and theoretical activities.

Recently, efforts have been focused on achieving THz detection using the standard, low-cost, complementary metal-oxide-semiconductor (CMOS) technology. In the case of communications, integration in CMOS technology could permit the entire receiver to be included easily in the chip, and ensures a low production cost. The low cost permits us also to imagine a large diffusion of a new generation of commercial devices, or, in turn, the design of large arrays or panels of detectors for a large area detection approach in order to achieve high sensitivity.

Until now, the explanation for the high-frequency detection by MOS field-effect transistors (MOS-FET) [4,5] has been based on the plasma wave detection theory [6]. In this

approach, it is assumed that the THz radiation generates waves of carriers in the 2D electron gas of the inversion layer, when a high-frequency electric potential is applied between the gate and source electrodes of a MOS-FET. Nonlinearities in the semiconductor equations convert these oscillations into a DC voltage. To increase the detector responsivity, this approach indicates that a strong downscaling of the gate length is necessary [7].

A recent work [8] evaluated the response characteristics of plasmonic terahertz field effect transistors on the base of this model. In the paper, the transistor response was calculated in two different regimes, with femtosecond and picosecond pulses, respectively. The calculation showed that the plasma wave may travel along the channel with different oscillatory decay processes, in the two cases, respectively, and the response time in the long pulse mode was significantly higher than that under the short pulse conditions.

A completely different approach to the self-mixing process has been developed in [9]. This new approach was also applied to the study of the double-barrier structure suitable for high-frequency radiation detection [10]. A preliminary indication of a possible application to the FET structure was given in [11]. The new approach shows how self-mixing occurs mainly in the semiconductor regions where barriers of potential are present, once the barriers are crossed by the RF electric field. In particular, in the MOS transistor structure, rectification occurs at the barrier between the channel and the doped region of the source contact. In this structure, the nonlinear transport of the majority carriers gives rise to their entrainment against the barrier, with the formation of a dipole of charge, and the generation of a potential.

The rectified potential then propagates along the channel of the transistor to reach the drain region and propose a voltage at the drain contact, and a current outside the structure. A rectified voltage/current can be observed also at the gate electrode, through the oxide capacitance [12]. Naturally, the voltage/current at the gate will be transient, due to the presence of a capacitance in series. Depending on the structure of the semiconductor device, on the channel resistance and on the parasitic capacitances, the transient time at the gate and at the drain can be dramatically different.

Numerical simulations allow us to evaluate the delay due to the signal propagation from the self-mixing dipole along the structure, as far as the electrodes. Nevertheless, the origin of the signal, i.e., the establishment of the self-mixing voltage due to the rectification of the THz radiation, to date can be only inferred by an analytical approach. Simulations indeed can describe the generation of harmonics by the harmonic balance analysis, in particular, of the zero-order harmonic which describes the rectification effect. Nevertheless, this analysis gives results in the steady-state condition; in principle, after that an infinite time has elapsed from the application of the radio frequency.

In this work, we propose an analytical method to calculate the transient of the photovoltage. We in particular further develop the analytical model proposed in [13] to describe the THz rectification in the MOS capacitance. As a structure for the calculation, we consider again the depletion zone of the semiconductor under the oxide, assuming it as a general model of a depletion in the presence of a barrier in a semiconductor. The developed model will provide an analytical solution of the growth transient of rectified potential.

The original model formulated in [13] was based on the hydrodynamic semiconductor equations solved for the small-signal approximation, and depicted the THz modulation mechanisms of the charge in the potential barrier. The model dramatically changed the paradigm assumed in the plasma wave model [6], where the modulation of carriers was studied in the channel, and under the RF effect of the gate potential. This new approach explains in particular the occurrence of the self-mixing process, the detection capability of the structure, and its frequency dependence. In this paper, we solve the equations in transient conditions. The analytical solution of the carriers and potential distribution within the semiconductor converge, for an infinite time, toward the steady-state solution formerly calculated.

The model in [13] was solved in steady-state conditions; the model proposed in this paper studies the transient of the formation of the photovoltage. The set of the equations

and the assumed structure, the depletion layer in a semiconductor barrier, are the same, but include both space and time as variables.

2. Analytical Model

We assume the structure of an MOS capacitance as reported in Figure 1. In the structure, we consider the depletion region with the thickness w. An abrupt edge is assumed at the edge of the depletion region, at x = 0. At the same edge, it is assumed that the ohmic contact (body) is placed. The oxide region has a thickness of d_{ox}.

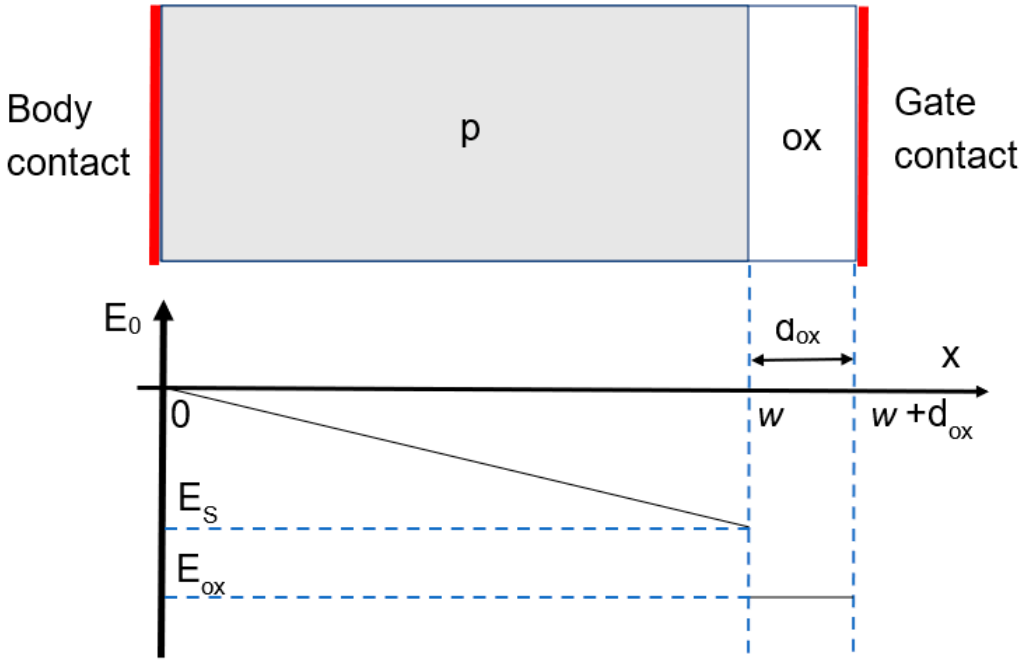

Figure 1. The studied semiconductor structure and a plot of the electric field distribution.

2.1. Polarization Conditions

We assume a polarization voltage V_G is applied between the gate and the body. In the following analysis, the gate voltage will be indicated as the voltage over the flat band condition, V_{FB}.

The electric field in the structure is expressed as:

$$E_0(x) = \frac{q}{\epsilon_s} N_A \, x \tag{1}$$

where ϵ_s is the dielectric constant of the semiconductor, and N_A is the doping density. q is the electron charge. Assuming zero potential at $x = 0$, within the depletion region, the potential varies as:

$$\phi(x) = \frac{1}{2} \frac{q}{\epsilon_s} N_A \, x^2 \tag{2}$$

Assuming the thermal equilibrium condition for the carriers, the equilibrium hole density is given by:

$$p_0(x) = p_{p0} e^{-\frac{\phi(x)}{V_T}} \tag{3}$$

where p_{p0} is the equilibrium hole density in the bulk region, thus equal to the doping value N_A; $V_T = \frac{k_B T}{q}$, k_B is the Boltzman constant; and T is the absolute temperature.

2.2. Radiofrequency Equations

We consider the following formulation of the hydrodynamic semiconductor equations:

$$\frac{\partial \phi}{\partial x} = -E \tag{4}$$

$$\frac{\partial E}{\partial x} = \frac{q}{\varepsilon_S}(p - n - N_A) \tag{5}$$

$$\frac{dp}{dt} = -\frac{\partial p v_p}{\partial x} + D_p \frac{\partial^2 p}{\partial^2 x} \tag{6}$$

$$\frac{\partial v_p}{\partial t} = -v_p \frac{\partial v_p}{\partial x} + \frac{q}{m_p} E - \frac{v_p}{\tau_p} \tag{7}$$

As given by the Poisson, Gauss, and continuity of holes equations, respectively, as extensively discussed in [13], while Equation (7) is the Euler equations in the approximation adopted by [6]. The self-mixing effect occurs within the majority carriers; thus, we study only the holes, which are majority carriers in the assumed structure. For the same reason, generation–recombination thus is not considered. All the physical quantities in these equations are considered as composed of an equilibrium state, plus eventual variations. We consider first a sinusoidal voltage drop, $V_G(t) = \hat{V}_G e^{j\omega t}$, applied to the gate, as the applied RF.

Following [13], we assume that the amplitude of the variations of the electric field within the depletion region does not depend on the position. As a direct consequence, the first-order holes' velocity variation is considered constant in space, while it is sinusoidal in time, superimposed onto the steady-state value: $v_p(t) = v_{p0}(x) + \hat{v}_p e^{-j\omega t}$. With this assumption, Euler's equation in the small-signal approximation leads to the determination of an equivalent, frequency-dependent mobility, mobility [13]:

$$\mu_p{}' = \frac{\frac{q}{m_p}}{j\omega + \frac{q}{\mu_p m_p}} \tag{8}$$

where μ_p and m_p are, respectively, the steady-state mobility and the effective mass of the holes. The solution of the continuity Equation (6) in steady-state conditions, thus assuming as null the time derivative, leads to a particular solution, which represents the variation of the majority carriers within the barrier at the end of the rectification process [13]:

$$\hat{p}(x) = \frac{\mu_p{}'}{\frac{D_p}{V_T} + \frac{j\omega}{\frac{q}{\epsilon_s} N_A}} \frac{p_{p0}}{V_T} e^{-\frac{\phi(x)}{V_T}} \hat{E} \tag{9}$$

The hole density variations enter into the nonlinear term in Equation (6). The time average of the carrier fluxes gives rise to a steady-state self-mixing term, $J_{SM} = q\langle p v_p \rangle$, which introduce a nonhomogeneous term in the DC current balance equations. The nonhomogeneous term has the form:

$$J_{SM}(x) = q\langle p(x) v_p \rangle = q \frac{\left|\mu_p{}'\right|^2 \hat{E}}{\sqrt{\left(\frac{D_p}{V_T}\right)^2 + \left(\frac{\omega}{\frac{q}{\epsilon_s} N_A}\right)^2}} \frac{p_{p0}}{V_T} e^{-\frac{\phi(x)}{V_T}} x = J_0 \, e^{-\frac{\phi(x)}{V_T}} x \tag{10}$$

2.3. Transient Evolution toward the Steady State

Expression (10) defines a forcing term arising into the semiconductor barrier due to the interaction of the electromagnetic field with the majority carriers, according to the nonlinear semiconductor equations. This term is generated within one single RF period. With the radiation in the THz range, the onset of the forcing term can thus be considered

as instantaneous with respect to the establishing of a potential in the structure. For the calculation of the potential transient across the barrier, we now evaluate the time-dependent solution of the differential Equation (6). The calculation is therefore not performed either in the THz regime, or in steady-state conditions, but, rather, the variation of the quantities in the semiconductor structure in response to the onset of the self-mixing effect is calculated.

Each of the quantities in Equation (6) must be considered as the sum of a zero-order term plus a variation term: $p = p_0 + \widetilde{p}$, $v_p = v_{p0} + \widetilde{v}_p$, where $\widetilde{p}$ and $\widetilde{v}_p$ are now the searched time-dependent densities of the holes and hole velocity, respectively. In determining the transient variations, unlike for the RF calculus, there is no external forcing generator; thus, the first-order amplitude of variation of the electric field, $\widetilde{E}$, cannot be neglected. Assuming the equilibrium condition among the different term, and neglecting the higher-order terms, Equation (6) can be rewritten for the small variations as:

$$\frac{d\widetilde{p}}{dt} = -\frac{\partial \widetilde{p}\widetilde{v}}{\partial x} + D_p \frac{\partial^2 \widetilde{p}}{\partial^2 x} = -\frac{\partial\left[p_0 \mu_p \widetilde{E} + \widetilde{p}\mu_p E_0\right]}{\partial x} + D_p \frac{\partial^2 \widetilde{p}}{\partial^2 x} + J_{SM} \tag{11}$$

Following a methodology developed in [13], we search solutions in the asymptotic approximation; i.e., we evaluate the solution obtained by one (in one case, two) of the terms in (11), assuming that the others could be neglected. This approach follows a technique commonly adopted for the solution of semiconductor equations, e.g., in the p–n junction. After the calculation, a comparison between the different solutions permits us to evaluate the entity of the approximation, choosing which one, among the examined terms, is actually ruling the behavior of the structure.

As a first step, we neglect the effect of the electric field variation, $\widetilde{E}$. Equation (11) thus reduces to:

$$\frac{d\widetilde{p}}{dt} = -\frac{\partial\left[\widetilde{p}\mu_p E_0\right]}{\partial x} + D_p \frac{\partial^2 \widetilde{p}}{\partial^2 x} + J_{SM} \tag{12}$$

Since the forcing term, J_{SM}, is not time-dependent, we search for a homogeneous transient solution. We write the homogeneous equation substituting the value of the DC electric field in the barrier as described in Equation (1):

$$\frac{d\widetilde{p}}{dt} = -\frac{\partial\left[-\widetilde{p}\mu_p \frac{q}{\epsilon_s} N_A x\right]}{\partial x} + D_p \frac{\partial^2 \widetilde{p}}{\partial^2 x} \tag{13}$$

Searching for a solution with separate variables in the form:

$$\widetilde{p}(t,x) = e^{-\propto t}\, \chi e^{-\frac{\phi(x)}{V_T}} x \tag{14}$$

with χ as a constant, we can write:

$$\alpha \chi e^{-\frac{\phi(x)}{V_T}} x = \chi \mu_p \frac{q}{\epsilon_s} N_A \frac{\partial\left[e^{-\frac{\phi(x)}{V_T}} x^2\right]}{\partial x} + D_p \chi \frac{\partial^2 e^{-\frac{\phi(x)}{V_T}} x}{\partial^2 x} \tag{15}$$

Using the potential expression as defined in Equation (2), we may obtain the following intermediate expression:

$$\begin{aligned} \alpha \chi e^{-\frac{\phi(x)}{V_T}} x = \chi \mu_p \tfrac{q}{\epsilon_s} N_A \left[-\tfrac{1}{V_T} e^{-\frac{\phi(x)}{V_T}} \tfrac{q}{\epsilon_s} N_A\, x^3 + e^{-\frac{\phi(x)}{V_T}} 2x\right] \\ + D_p \chi \left[-\tfrac{1}{V_T} e^{-\frac{\phi(x)}{V_T}} \tfrac{q}{\epsilon_s} N_A x \left(-\tfrac{1}{V_T}\, \tfrac{q}{\epsilon_s} N_A\, x^2 + 1\right) - e^{-\frac{\phi(x)}{V_T}}\, \tfrac{1}{V_T}\, \tfrac{q}{\epsilon_s} N_A\, 2x\right] \end{aligned} \tag{16}$$

The spatial dependence of both sides of Equation (16) is equal; thus, we finally obtain:

$$\alpha = -\mu_p \frac{q}{\epsilon_s} N_A \tag{17}$$

Imposing the time boundary condition, $\widetilde{p}(0,x) = 0$, to the whole solution of the first-order time-dependent equation, and thus, homogeneous term plus the forcing term, we obtain:

$$\widetilde{p}(t,x) = \left(1 - e^{-\propto t}\right) J_0 \, e^{-\frac{\phi(x)}{V_T}} x \tag{18}$$

Expression (18) describes the transient from zero toward the steady-state solution, which coincides with the values formerly calculated in [13].

Expression (18) is obtained considering only two (the second and third) of the three terms present in the differential Equation (11); it represents an asymptotic solution, which is valid only if the contribution of the neglected first term is negligible. We now calculate the solution assuming as dominant the first term, containing the variation of the electric field $\widetilde{E}(x)$. Equation (11) becomes:

$$\frac{d\widetilde{p}(x)}{dt} = -\frac{\partial\left[\mu_p p_0 \widetilde{E}(x)\right]}{\partial x} + \frac{\partial J_{DC}(x)}{\partial x} \tag{19}$$

Since the forcing term is not time-dependent, we search for a homogeneous transient term.

$$\frac{d\widetilde{p}(x)}{dt} = -\frac{\partial\left[\mu_p p_0 \widetilde{E}(x)\right]}{\partial x} \tag{20}$$

We search for a solution with separate variables in the form

$$\widetilde{p}(t,x) = e^{-\propto t} p(x) = e^{-\propto t}(A + Bx) \tag{21}$$

Expressing the electric field by the Poisson equation, and performing the derivative, we obtain the same time exponent of the first asymptote:

$$\propto = -\mu_p \frac{q}{\epsilon_S} p_{p0} = -\mu_p \frac{q}{\epsilon_S} N_A \tag{22}$$

We substitute in expression (19) the known spatial dependences of the steady-state distributions of the holes in the depletion region, following Equation (3). Imposing the time boundary condition $\widetilde{p}(0,x) = 0$ to the whole solution of the first-order time-dependent equation, and thus, homogeneous term plus the forcing term, we obtain:

$$\widetilde{p}(t,x) = \left(1 - e^{-\propto t}\right) \frac{J_0}{\mu_p p_{p0}} \left(-\frac{\in_S}{q} + \frac{N_A}{V_T} \frac{3}{2} x\right) \tag{23}$$

Both of the two different asymptotes can be expressed by separate variables, with the same time-dependence; both spatial dependencies remain constant during the time evolution. Therefore, the comparison and the choice between the two solutions can be performed following the method already demonstrated in the steady-state condition in [13]. The method considers calculating the solution given by the different solutions, and comparing their effects as the electric potential required to obtain a total current that can equal the nonhomogeneous term. In [13], it has been demonstrated that the second asymptote, reported in Equation (23), is always negligible with respect to the first one, reported in Equation (18).

3. Results from the Model

The first asymptote, Equation (18), describes the formation of a dipole. In the examined case with the p-doped substrate, the holes are pushed by the nonlinear interaction against the barrier, creating an accumulation within the depletion region. The function indicates that this accumulation has a maximum within the depletion layer, and is described by Figure 2, where the distribution of the hole variation is calculated for different doping concentrations. The increase of holes corresponds to a transport of the carriers from the

substrate; thus, an equivalent negative charge must be considered at the edge of the region, at $x = 0$. This effect substantially describes the formation of a dipole.

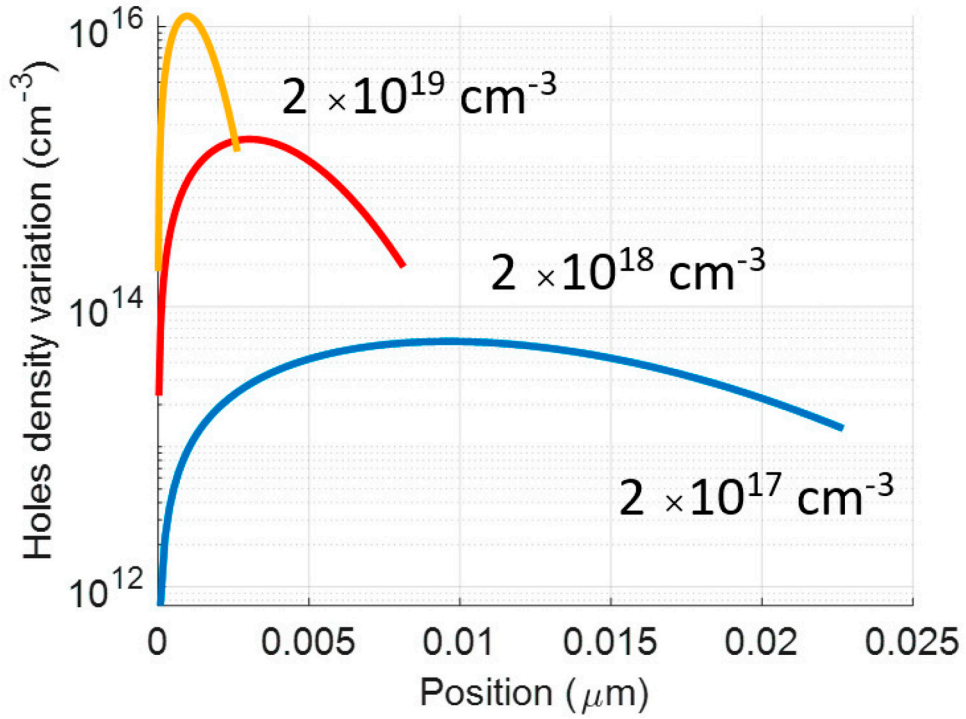

Figure 2. Distribution of the density of hole variation within the depletion zone, as a function of the doping concentration of the substrate.

This result is obtained by the abrupt edge approximation; nevertheless, a similar result is obtained by numerical simulations, in which the limit of the depletion edge is continuously degrading toward the substrate. In Figure 3, we show the variation of hole density obtained by numerical calculation, in the depleted region under an MOS structure. For the chosen color scale, red corresponds to an increase of the holes density, while the blue color corresponds to a decrease.

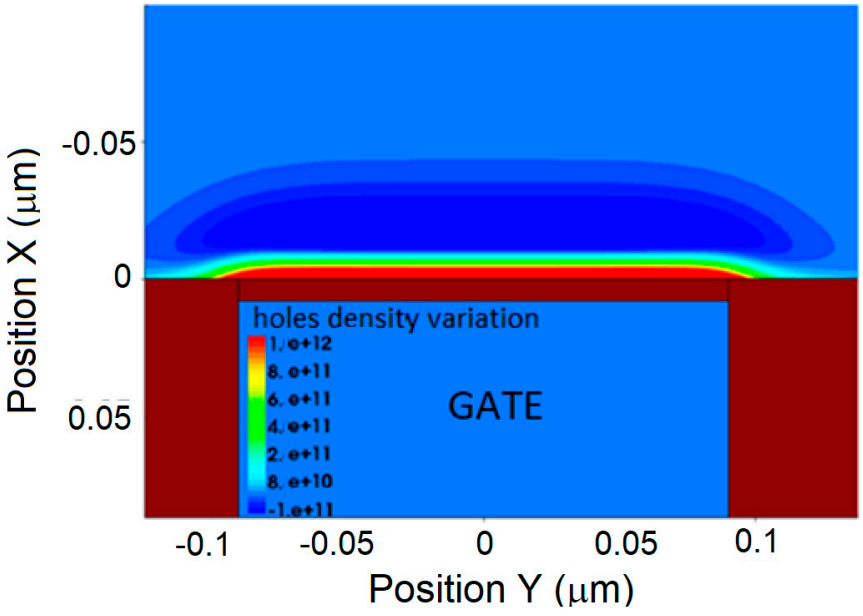

Figure 3. Results from the harmonic balance simulation of self-mixing. Distribution of DC charge variation (the bar scale is cm^{-3}), showing positive (red) and negative (blue) variations of the holes density.

The formation of a dipole within the depletion region, along the line of the junction, is a characteristic of the self-mixing. It can be found also in the p–n junction, in MOSFET [11,12], and in double barriers [10]. In [14], the formation of the dipole appears in the structure of a junctionless field-effect transistor (JL-FET) [15], along the barrier between the source doping and the channel.

Figure 4 reports the dependence of the absolute value of the self-mixing photovoltage at the silicon dioxide interface (x = w) with respect to the gate voltage at three different substrate doping concentrations (2×10^{17}, 2×10^{18}, and 2×10^{19} cm^{-3}), all simulated at 1 THz. The detector is assumed to be placed at the air gap on an antenna. The effect of the collected radiation is represented by the RF applied voltage; in this case, we assumed it to have the value of 1 mV. The simulations present at any doping level a behavior with a bell shape. Each distribution presents a maximum. This observation permits us to offer a qualitative interpretation of the proposed model. At low gate voltages, the depletion condition produces a low steady-state electric field. Since this parameter represents a determinant element for the generation of the self-mixing process, at zero gate voltage, in any condition, the electric field is null, and consequently the self-mixing current term is null in Equation (10).

Increasing the gate voltage, we see that the photovoltage decreases. From Equation (10), we find that the self-mixing current term depends on the potential inside the depletion region; its maximum moves toward the depletion edge, where the electric field is lower, and consequently the self-mixing voltage effect decreases.

From Figure 4, we see that the absolute value of the gate voltage at which the maximum occurs increases with the substrate doping. Nevertheless, the peak value of the photovoltage presents a maximum at a given substrate doping. The doping value at which the peak occurs depends on the frequency of the exiting RF radiation [13].

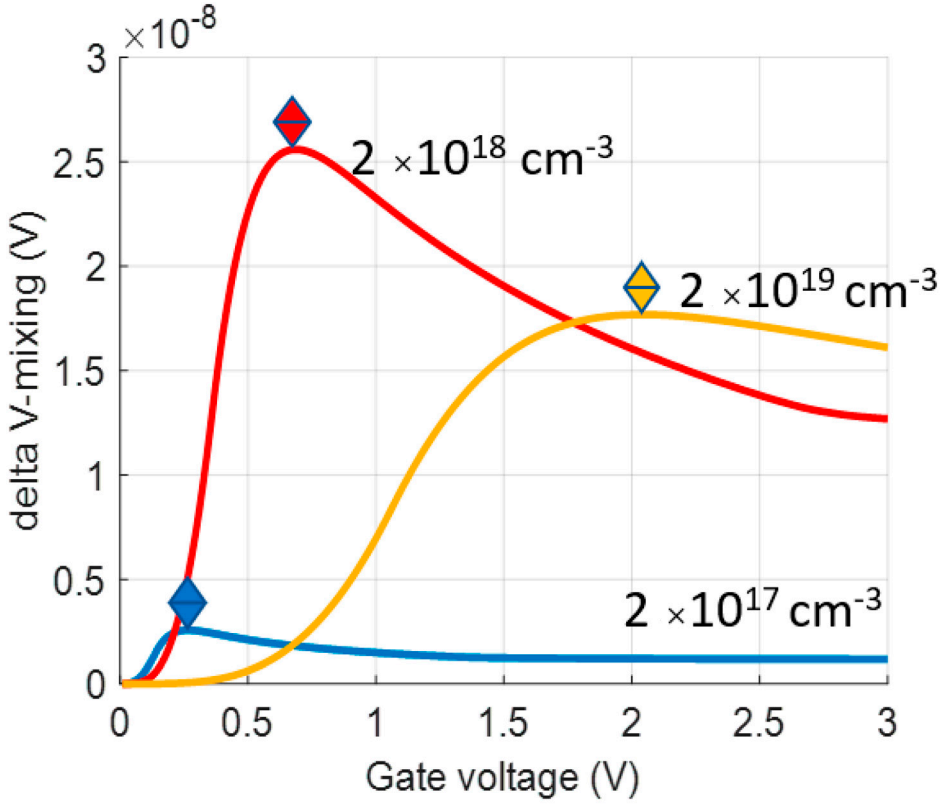

Figure 4. Absolute value of self-mixing voltage generated within the structure, calculated at 1 THz, for different values of the substrate doping. The diamonds indicate the maximum. The potential distributions in Figure 5 are calculated respectively at the corresponding gate voltages.

Figure 5 reports the distribution of the potential generated by the self-mixing process within the depletion region, calculated with different doping concentrations and at different gate voltages, with values corresponding to the peaks in Figure 4, in particular, for $N_A = 2.10^{17}$, $V_G = 0.25$ V; $N_A = 2.10^{18}$, $V_G = 0.70$ V; and $N_A = 2.10^{19}$, $V_G = 2.02$ V. This figure permits us to evaluate how the photovoltage generation distributes within the semiconductor substrate. The depletion region naturally is shorter at the higher doping concentration. It is worth noticing that the maximum of the photovoltage occurs at the intermediate value of doping, 2.10^{18}. The right side of each curve is interrupted, corresponding with the silicon/silicon dioxide interface. After this interface, the potential drops linearly to zero within the oxide since the gate is grounded. This behavior is not reported. The figure shows that a relevant portion of the rectification potential drops across the oxide layer, thus accumulating charge, and thus allowing an external detection also at the gate.

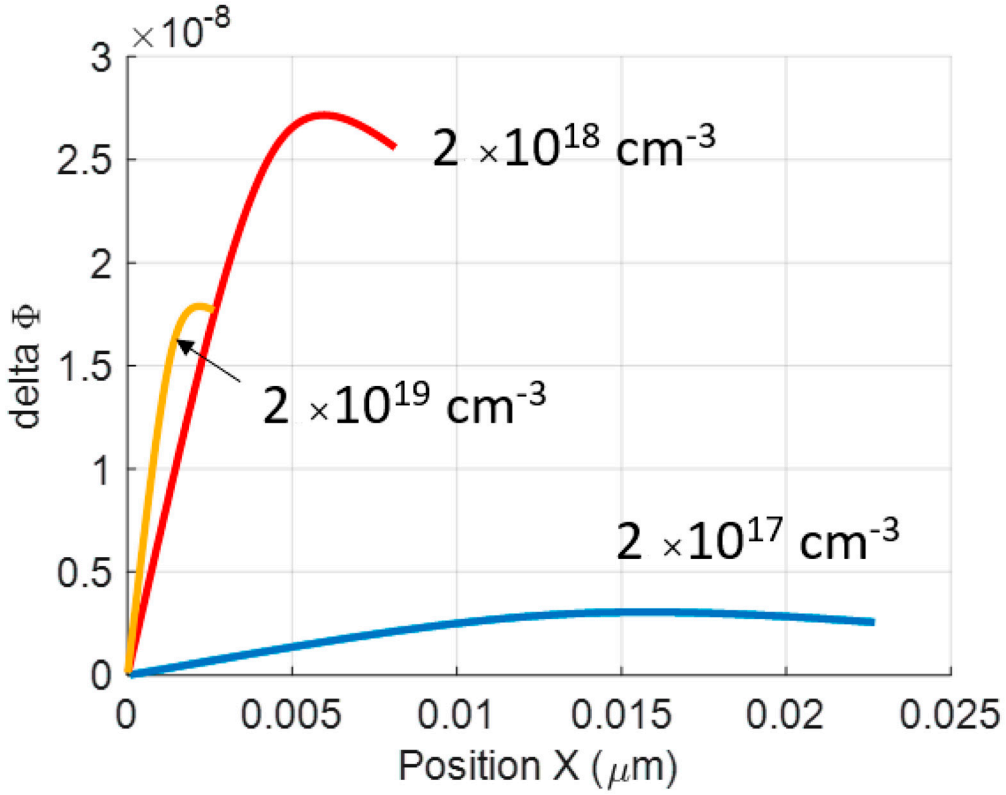

Figure 5. Absolute value of self-mixing potential within the depletion region, calculated at 1 THz, for different values of the substrate doping, at different gate voltages corresponding to the peaks in Figure 4, respectively, VG = 0.25 V, VG = 0.70 V, and VG = 2.02 V.

Figure 6 reports the dependence on the characteristic time constant, respectively, for the holes and electrons, as a function of the doping density, following Equation (22). Based on this equation, the response time could be extremely short. A limitation of the calculation should be considered if the assumption of the instantaneous generation of the forcing term, $J_{SM} = q\langle pv_p \rangle$, cannot be accepted. The term indeed is borne as the average, along, at least, the half-life period of the incoming radiation. Thus, the RF period itself limits the response time.

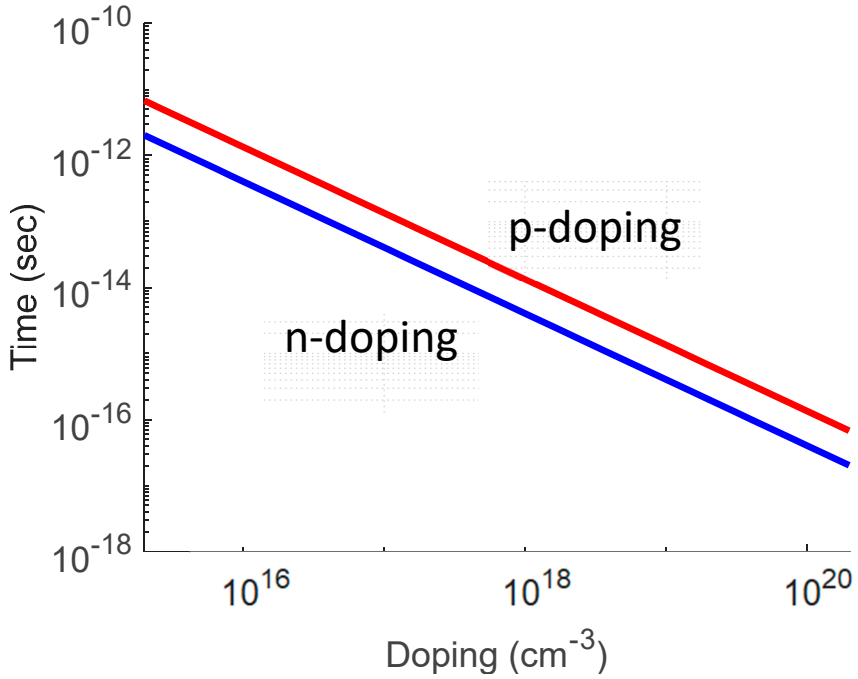

Figure 6. Time constant of the establishment of the self-mixing photovoltage as a function of the doping density, respectively, orange for p and blue for n doping.

4. Propagation of the Photovoltage within the Structure

A harmonic balance analysis gives results in the steady-state condition, in principle, after an infinite time has elapsed from the application of the radio frequency. This is the case, in particular, for the zero-order harmonic, which describes the rectification effect. Numerical simulations are obtained by TCAD [16]. Hydrodynamics equation analysis allows us to take into account the propagation within the structure, but the forcing term, generated within the depletion region of a barrier, cannot be included in the analysis. The harmonic balance analysis calculates the forcing term, but this result is not shared with the transient analysis. There will probably be in the future a development of the software, but, at the moment, this is not available.

We observe that the self-mixing effect generates a current as the forcing term, Equation (10), and that the response of the semiconductor structure to this current is the formation of a charge dipole, distributed transversely to the barrier, along the depletion region crossed by the RF electric field. In order to overcome the simulation limit, in this last paragraph, we mimic the formation of the dipole, introducing within the structure a couple of parallel plate contacts, positioned in particular within the depletion region of the barrier involved in the self-mixing effect. As a test case, we performed simulations on a structure known as Junctionless FET (JL-FET) [14]. Figure 7 reports the doping distribution of the structure. Figure 8 reports the distribution of the RF potential inside the structure. We assume a 3.5 µm gate width, and a 500 nm gap between the polySi gate and source/drain n^+ diffusions. The channel is n-type, doped 2.10^{16} cm^{-3}, while doping n^+ at the source, and the drain diffusions is 1.10^{20} cm^{-3}. The SOI device layer is 170 nm and the gate oxide is 26 nm thick. We assume that an RF at 1 THz is applied between the gate and the grounded source.

The structure analyzed is very large; nevertheless, the rectification effect appears quite strong, and, thus, it is almost ideal in order to highlight the genesis of the self-mixing effect.

Due to the doping structure under the contacts, two n^+/n^- junctions are present between the contacts and the channel. The two depletion regions are normal to the semiconductor surface. In particular, the depletion region toward the source is crossed orthogonally by the RF electric field.

In [16], the detail of the formation of the photovoltage inside the structure is presented. In particular, the TCAD simulation shows that a charge dipole arises along the barrier between the source doping and the channel. Simulations have been obtained using a harmonic balance analysis of the TCAD simulator, which takes into account in particular the nonlinearities present in the semiconductor equations, thus reproducing the self-mixing effect. We extracted the variations of electrons due to the self-mixing, indicated in the following with the label A1, subtracting from the harmonic balance solution of the electron density, C0, the distribution at rest. Figure 9 reports the quantity A1, and shows the formation of the charge dipole with the bias voltage at the gate VG = −1.9 V, which corresponds to a partially depleted channel.

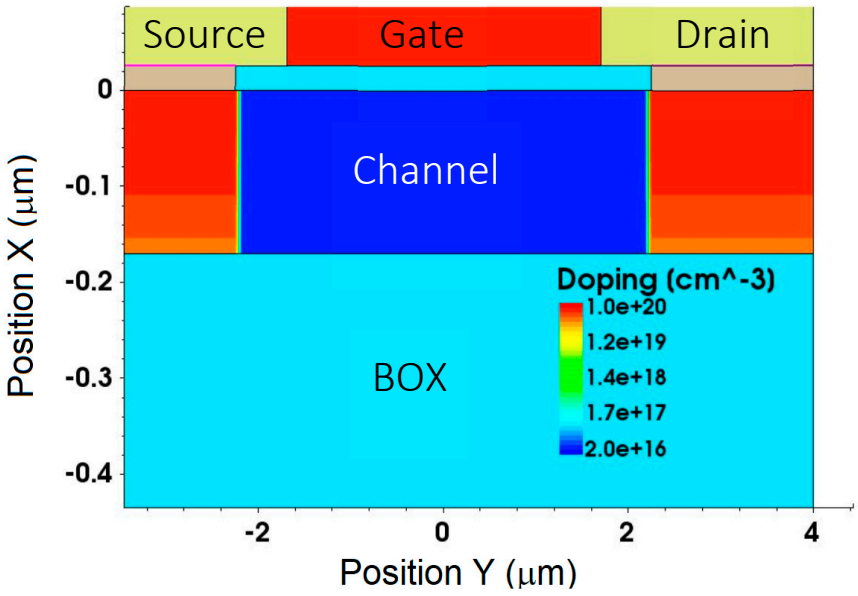

Figure 7. Schematic structure of the doping distribution in the JL-FET structure.

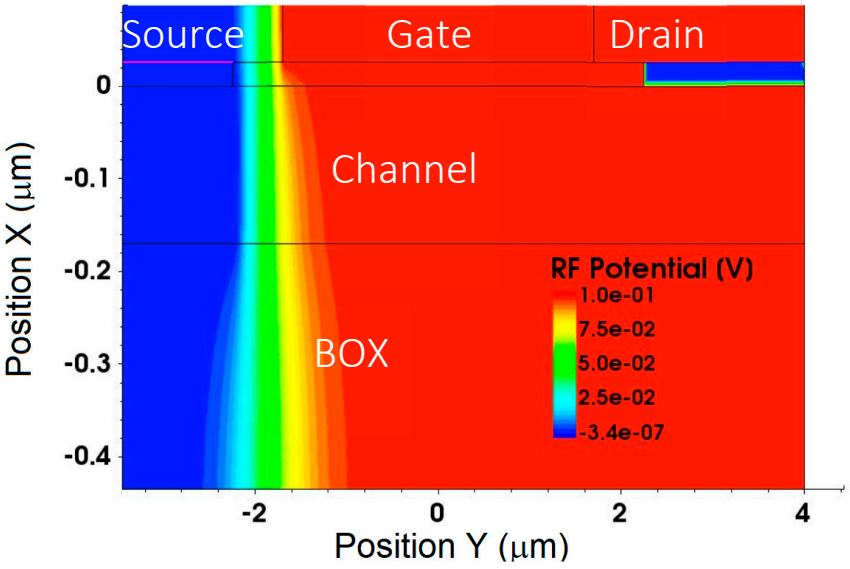

Figure 8. RF potential distribution with 100 mV applied between gate and source.

Coherent with the predictions, the dipole is transversal to the junction, normal to the surface, and is approximatively homogeneous along its entire extension.

In the transient analysis, we simulated the effect of the formation of the dipole introducing two electrodes, embedded within the source/channel barrier. We choose the

position and the extension of the contacts following the results of the simulations, placing the electrodes within the barrier, parallel to the junction. The contacts have the same length as the junction, and are spaced 10 nm apart. Since they are placed along an equipotential direction, in principle, these electrodes do not alter the shape of the barrier. We impose, among the properties of the electrodes, the characteristic of no recombination, so the presence of the electrodes does not alter the density of the minority carriers.

We apply a step current generator between the two electrodes, imitating the current forcing term. As a result, a voltage arises between the two electrodes. The rise time of this voltage is very fast, since a thin layer of a highly doped semiconductor separates the two. The rise of the voltage propagates along the semiconductor structure, reaching the external electrodes of the device, all placed in a short circuit condition, where we finally obtain a transient of the current.

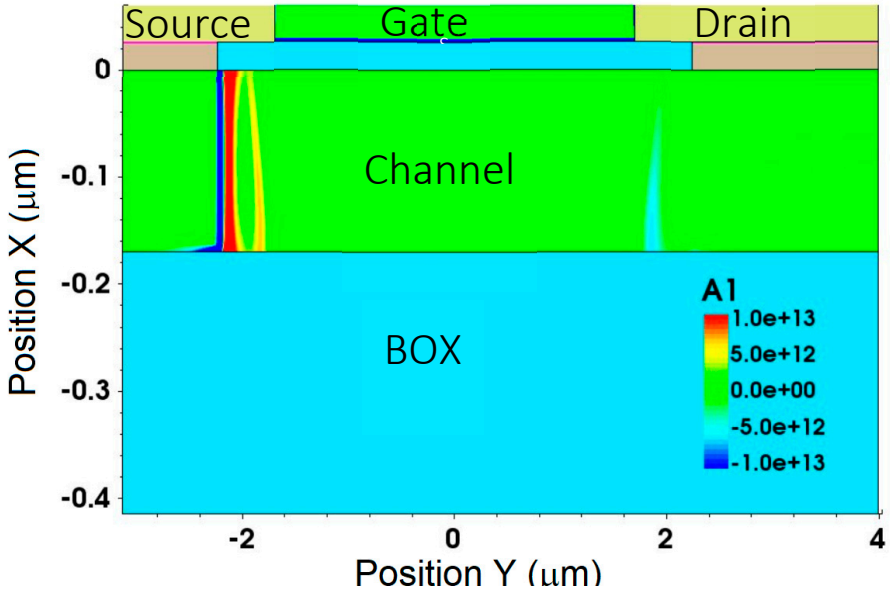

Figure 9. DC variation of the electron density due to the self-mixing effect.

In the simulation, internal electrodes are fed a 1 μA step of current. The generation of potential at the dipole produces a current along the channel, toward the drain. Simultaneously, there is an accumulation of charge at the oxide interface, which produces a transient current at the gate. Figure 10a,b reports the transient current, respectively, at the gate and the drain, under different values of the bias gate voltage, respectively, −1 V, 0 V, 0.0 V, and 2 V. In general, the peak of the current at the gate is two orders of magnitude larger than the current at the drain. The conductance of the channel, determined by the gate voltage, determines the transient length. A higher conductivity shortens the current pulse at the gate, and reduces the charging time of the parasitic capacitance, causing the current to reach the drain faster.

We must observe that a very wide structure has been taken for this case study, only justified by the need to identify easily the presence and the shape of the dipole generated by the self-mixing. The linear shape of the depletion region in the structure determines the linear shape of the dipole, and permits us to design very simply a couple of equivalent electrodes.

Even in the relaxed structure of the JL-FET, the response current through the gate capacitance is extremely fast. The current pulse is shorter than 100 ps. The current response to the drain is obviously longer, due to the presence of a channel resistance, and of the channel–gate and channel–substrate parasitic capacitances. An experimental evidence of the current response at the drain in JL-FET can be found in [15].

The simulations we just presented indicate clearly, in the opinion of the author, that the entire rectification process of the THz radiation within the MOS structure can be very fast, independently of the scaling node of the transistor. This awareness permits us to forecast

the possibility of using this structure for the detection of high-data-rate communications, using the THz carriers.

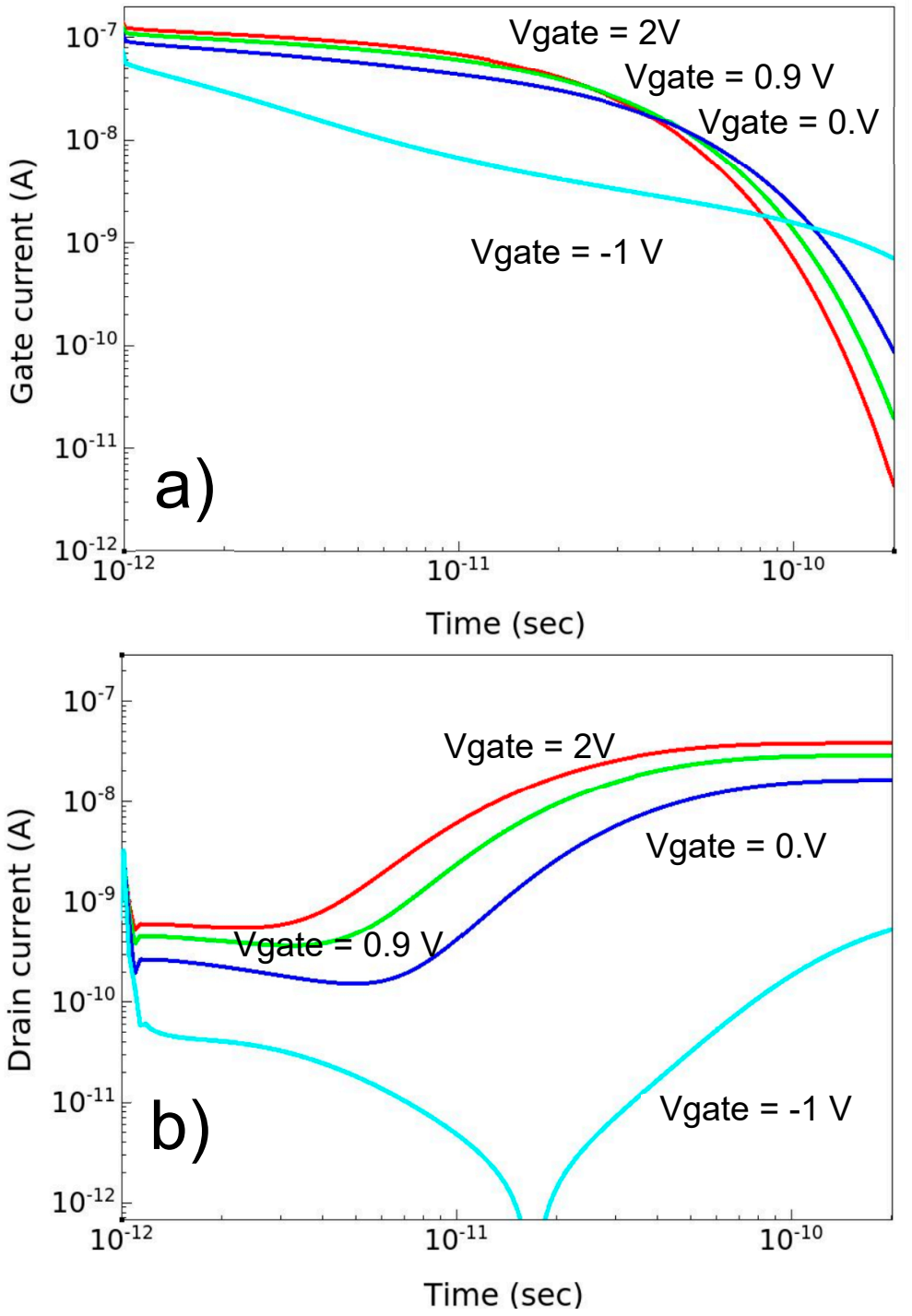

Figure 10. Simulations of the transient current in the JL-FET structure at four different values of the gate polarization, respectively, Vgate = 2 V, 0.9 V, 0 V, and −1 V: (**a**) current at the gate at the four biases; (**b**) current at the drain at the four biases.

5. Conclusions

This paper presented a new model of the transient of the rectification of the THz radiation process in an MOS structure. The model is based on the hydrodynamic semiconductor

equations, solved for the small-signal approximation, and leads to the determination of the time constant of the photovoltage growth.

The rectification process is not limited by the damping effect of the parasitic C_{GS} capacitance, since it is not related to the plasma waves in the channel. The self-mixing process arises indeed, due to the nonlinear effects of the carrier dynamics, within the depletion layers of any junction crossed by the RF electric field.

Numerical TCAD simulations extended the analytical results, allowing the determination of the current transient at the gate and source electrode of a structure. In particular, as an example of a general behavior, the simulations illustrated the THz modulation mechanisms of the charge in the depleted region of a JL-FET, showing that a detection through the current at the gate can be extremely fast, not depending on the transistor dimensions. The model proposed substantially offers a completely new insight on the THz detection process of fast signals.

Funding: Italian PNRR, Project Restart-T-Next.

Data Availability Statement: Data sharing not applicable.

Conflicts of Interest: The author declares no conflict of interest.

References

1. Nagatsuma, T. THz communication systems. In Proceedings of the Optical Fiber Communication Conference (pp. Tu3B-1), Los Angeles, CA, USA, 19–23 March 2017.
2. Tohme, L.; Ducournau, G.; Blin, S.; Coquillat, D.; Nouvel, P.; Pénarier, A.; Lampin, J.F. 0.2 THz wireless communication using plasma-wave transistor detector. In Proceedings of the 2013 38th International Conference on Infrared, Millimeter, and Terahertz Waves (IRMMW-THz), Mainz, Germany, 1–6 September 2013.
3. Al Hadi, R.; Sherry, H.; Grzyb, J.; Baktash, N.; Zhao, Y.; Öjefors, E.; Pfeiffer, U. A broadband 0.6 to 1 THz CMOS imaging detector with an integrated lens. In Proceedings of the 2011 IEEE MTT-S International Microwave Symposium, Baltimore, MD, USA, 5–10 June 2011; pp. 1–4. [CrossRef]
4. Lisauskas, A.; Pfeiffer, U.; Öjefors, E.; Bolìvar, H.P.; Glaab, D.; Roskos, G.H. Rational design of high-responsivity detectors of terahertz radiation based on distributed self-mixing in silicon field-effect transistors. *J. Appl. Phys.* **2009**, *105*, 114511. [CrossRef]
5. Corcos, D.; Brouk, I.; Malits, M.; Svetlitza, A.; Stolyarova, S.; Abramovich, A.; Nemirovsky, Y. The TeraMOS sensor for monolithic passive THz imagers. In Proceedings of the 2011 IEEE International Conference on Microwaves, Communications, Antennas and Electronic Systems (COMCAS 2011), Tel Aviv, Israel, 7–9 November 2011; pp. 1–4. [CrossRef]
6. Dyakonov, M.; Shur, M. Detection, mixing, and frequency multiplication of terahertz radiation by two-dimensional electronic fluid. *IEEE Trans. Electron. Devices* **1996**, *43*, 380–387. [CrossRef]
7. Schuster, F.; Coquillat, D.; Videlier, H.; Sakowicz, M.; Teppe, F.; Dussopt, L.; Knap, W. Broadband terahertz imaging with highly sensitive silicon CMOS detectors. *Opt. Express* **2011**, *19*, 7827–7832. [CrossRef] [PubMed]
8. Zhang, Y.; Shur, M.S. Ultrashort Pulse Detection and Response Time Analysis Using Plasma-Wave Terahertz Field-Effect Transistors. *IEEE Trans. Electron. Devices* **2020**, *68*, 903–910. [CrossRef]
9. Varlamava, V.; de Amicis, G.; del Monte, A.; Perticaroli, S.; Rao, R.; Palma, F. CMOS-Compatible Room-Temperature Rectifier Toward Terahertz Radiation Detection. *J. Infrared Millim. Terahertz Waves* **2016**, *37*, 737–752. [CrossRef]
10. Palma, F.; Rao, R. A Model of High frequency Self-Mixing in Double-Barrier Rectifier. *J. Infrared Millim. Terahertz Waves* **2018**, *39*, 422–438. [CrossRef]
11. Palma, F.; Rao, R. Terahertz Detection in MOS-FET: A new model by the self-mixing. In Proceedings of the 2018 43rd International Conference on Infrared, Millimeter, and Terahertz Waves (IRMMW-THz), Nagoya, Japan, 9–14 September 2018. [CrossRef]
12. Palma, F. New Insight on Terahertz Rectification in a Metal–Oxide–Semiconductor Field-Effect Transistor Structure. *Electronics* **2020**, *9*, 1089. [CrossRef]
13. Palma, F. Self-mixing model of terahertz rectification in a metal oxide semiconductor capacitance. *Electronics* **2020**, *9*, 479. [CrossRef]
14. Palma, F.; Zagrajek, P.; Zaborowski, M.; Marczewski, J.; Di Tomassi, G.; Mazzetta, I. Fast Time Response of THz detection in JLFET. In Proceedings of the 46th International Conference on Infrared, Millimeter and Terahertz Waves (IRMMW-THz), Chengdu, China, 29 August–3 September 2021. [CrossRef]
15. Zagrajek, P.; Danilov, S.N.; Marczewski, J.; Zaborowski, M.; Kolacinski, C.; Obrebski, D.; Ganichev, S.D. Time resolution and dynamic range of field-effect transistor–based terahertz detectors. *J. Infrared Millim. Terahertz Waves* **2019**, *40*, 703–719. [CrossRef]
16. *Sentaurus Device, Synopsys User Manual, Version Y-2006.06*; Synopsys, Inc.: Mountain View, CA, USA, 2006.